Strojniški vestnik - Journal of Mechanical Engineering 70(2024)7-8, 381-391
© 2024 The Authors. CC BY 4.0 Int. Licensee: SV-JME
DOI:10.5545/sv-jme.2023.899
Original Scientific Paper
Received for review: 2023-12-16
Received revised form: 2024-04-12
Accepted for publication: 2024-06-19

Cargo E-Bike Robust Speed Control Using an MPC Battery Thermal Lumped Model Approach

Mehmet Onur Genç
Bursa Technical University, Department of Mechatronics Engineering, Turkey

Cargo e-bikes are expected to convey heavy loads in all aspects of daily life. Also, these vehicles are expected to maintain a consistent speed to meet mobility needs while optimizing the battery design. In this paper, a control model is developed to improve rotational speed motor control via the battery model predictive controller (MPC) thermal model designed based on experimental field test data. Experimental field tests are performed to provide the relation between battery surface and ambient temperatures in different road types and weight conditions. For this purpose, in different slope ranges, the pedal load/activity and voltage-current data are logged to use as experimental input in an MPC-integrated 1D model. To obtain the desired thermal conditions in the Li-Ion battery, the MPC battery thermal model is defined based on the thermal lumped model approach. In the next step, the generated MPC model is used as a function for longitudinal speed control in the MPC motor torque control model subjected to uncertain road disturbances. Then, the outputs of the control models are compared using the MPC parameters oc weight factors and prediction horizon. Thus, the speed control model for cargo e-bikes is presented with increased robustness using the MPC battery thermal lumped model approach considering energy and Li-Ion battery life-cycle efficiency methods regardless of driving performance needs.

Keywords: cargo e-bike, e-micromobility, MPC, robust control, road uncertainty, lumped thermal model, state-space modelling

Highlights

- *The new model is proposed for cargo e-bike speed control using the MPC battery thermal lumped model approach.*
- *The integrated robust speed control model is created by considering energy and battery life-cycle efficiency methods without taking driving performance needs into consideration.*
- *The thermal condition of the battery is controlled by using this method before the battery reaches unsafe temperatures.*
- *The lumped thermal model is used as the function of the longitudinal speed control model to provide thermally control-based driving.*
- *Sensitive weight factor selections have a significant effect on preventing overshoot within the robust control model, even if the same prediction horizon is used.*

0 INTRODUCTION

E-micromobility has significantly improved transportation in various areas. As a result, optimizing motor torque consumption becomes more important for energy-efficient driving of cargo e-bikes. This study approaches the research from an experimental and model development point of view. The experimental test gives the energy capacity related to internal heat-up conditions under different ambient temperatures. The study is constructed based on two different steps: experimental tests and control model development. The experimental tests also include two stages: thermal and electro-mechanical tests to provide inputs for control model development. In the first stage, the experimental tests are performed to observe the thermal conditions of the two different capacities of batteries to cover the variety and uncertainty to provide a robust control methodology. The second step of the study includes pedal load and current-voltage measurements based on the slope and road conditions, with the pedal load vs. current-voltage (Figs. 11 and 12) condition as model input. The increased scope of the experimental data is the input for an integrated robust MPC control model.

MPC controllers can also be used for non-linear system controls. In this study, a linear MPC controller is selected and used in the modelling studies. Learning state-space models have also been used in plant models in recent years. In these models, the plant outputs are estimated via a data-training process, and results are found via neural network processing [1]. These models are preferred and accompanied by MPC control models [2].

MPC has recently also been investigated and validated for the battery developments in literature. Battery life-cycle studies using MPC control methods mainly focused on thermal management to control the battery ageing process. Ma et al. [3] developed an MPC trajectory tracking control model providing optimized battery energy consumption. To provide the model, the lateral and longitudinal deviations are derived with state selection into the plant, and then the battery energy consumption model is produced within the loss function to be used in the optimizer. Surya et al. [4] studied the energy consumption control

*Corr. Author's Address: Bursa Technical University, Department of Mechatronics Engineering, Bursa, Turkey, onur.genc@btu.edu.tr

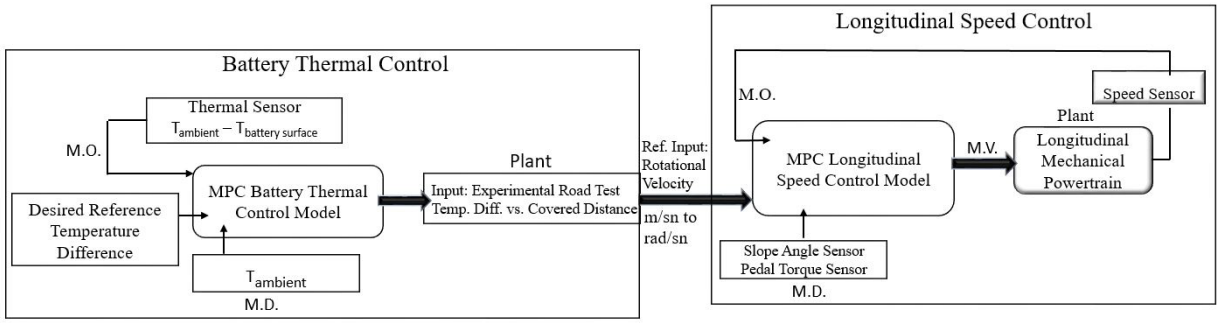

Fig. 1. *Proposed control model – battery MPC control model as input reference for longitudinal MPC speed control*

model development to improve battery management system (BMS) efficiency. In the study, they developed the optimization algorithm by considering the lump thermal model and used the base model to estimate battery surface temperature and battery core temperatures. Batiyah et al. **[5]** investigated a power management system (PMS) to provide optimized disturbances transients, overcharging the battery and effectively consuming the power. Masoudi and Azad **[6]** proposed a battery thermal management system (BTMS) for plug-in hybrid electric vehicles. They studied the non-linear model predictive control (NMPC) thermal controller for the system following the trajectory system. Shi et al. **[7]** studied an internal battery temperature estimator, developing an MPC controller for real-time state observer and Kalman filter.

A three-wheel cargo e-bike is instrumented and experimentally real-time observed to provide an MPC-integrated one-dimensional (1D) model (Fig. 1). As illustrated in Fig. 2, in discrete time variance, obtained measured data is processed via MPC optimizer to have a prediction in optimized levels.

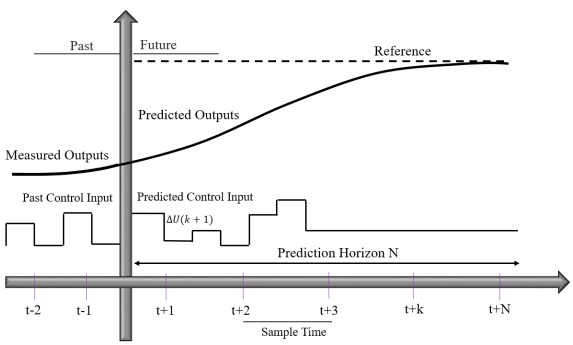

Fig. 2. *MPC operation chart*

Eq. (1) represents the reference value for the manipulated variable (M_V), Q, which stands for the weight factor for M_V data. U represents the input value, which is the input for the MPC controller. R is the weight factor for an input value and defines the effectiveness of the input factor in the control algorithm. The measured disturbances as input defined are indicated in U matrix; this enables visualizing the repercussions of the measured disturbances within the plant system **[8]**. Eq. (2) shows the discrete-time of the Loss function which is held to optimization. In this version, the matrix format is prepared, and the sum of the total values is calculated based on sample time during the total horizontal definition named N.

$$\int(x,u) = (x - x_{ref})Q(x - x_{ref})^T + RU^2, \tag{1}$$

$$\min U_1,..,U_N = J(x_k, U_k) = \sum_{i=1}^{N}\left[x(i)Qx^T(i) + U(i)RU^T(i)\right]. \tag{2}$$

Eq. (3) shows the state-space model in continuous time frame. In the MPC controller and optimization-based control algorithms, the calculations are done in a discrete-time system. Eq. (4) shows the discrete-time system definition based on k sample time.

$$\begin{aligned} \dot{x} &= [A][X] + [B][U], \\ y &= [C][X] + [D][U], \end{aligned} \tag{3}$$

$$\begin{aligned} x(k+1) &= A_d X(k) + B_d U(k), \\ y(k) &= C_x X(k) + B_k U(k). \end{aligned} \tag{4}$$

During the test, a three-wheeler e-bike was used (Fig. 3). During the experimental tests, the first gear was used, meaning 2:1 torque transmission from pedal torque. Due to the one-wheel torque transmission, e-bike dynamics are differentiated from two-wheelers, creating challenging control of steering due to the created continuous force on the right section of the bike. The left wheel is without power, so the unbalanced condition needs extra effort to control the bike. The used bike has a 26-inch (around 66 cm diameter) wheel dimension.

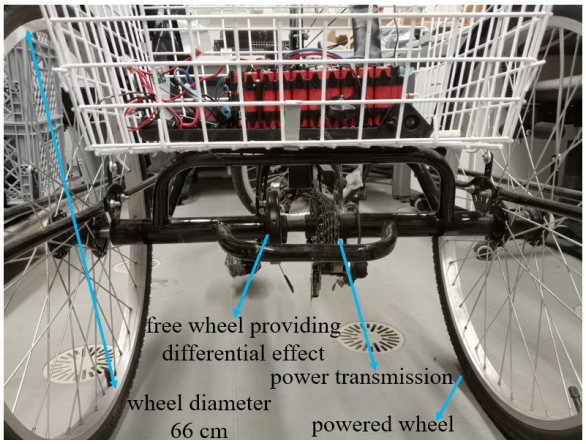

Fig. 3. *Three-wheeler powertrain chart*

Fig. 4 shows the instruments used and capacity details during experimental tests. The three-wheeler e-bike consists of a hub motor (36 V, 250 W continuous power, 35 Nm maximal torque), controller, and battery packets. Fig. 5 shows the general equipment and instrumentation places of the e-bike. The pedal load sensor is placed on the pedal, and thermal sensors and voltage-current recorder are placed at the rear carrier of the bike.

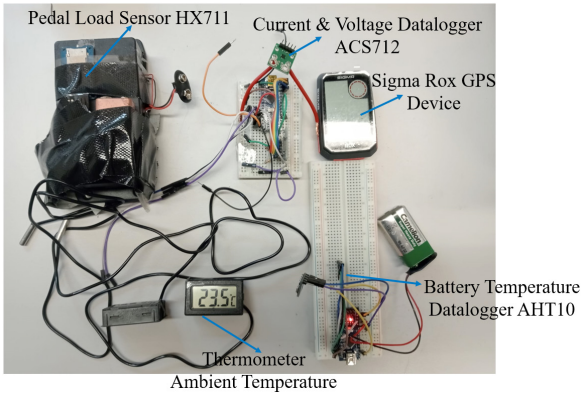

Fig. 4. *Instrument data used in the study*

Fig. 5. *Three wheelers e-bike using experimental tests*

1 THERMAL FIELD TESTS UNDER VARIABLE AMBIENT TEMPERATURES WITH DIFFERENT BATTERY CAPACITIES

During experimental tests, drives were performed with two different batteries with different energy capacities in two different test roads for each battery to increase the diversity and sensitivity of the control model robustness. Fig. 6 shows the handmade battery. The cells are designed as serial, with a total of 10 cells providing 36 V total nominal voltage (max. 42 V, 29-V cut-off voltage) and a total 3.2 Ah energy capacity due to serial connection. The second battery has a total of 40 cells with 13 Ah energy capacity with serial-parallel combinations. The cells also have 18650 geometrical dimensions and a 3.2 Ah unique cell capacity.

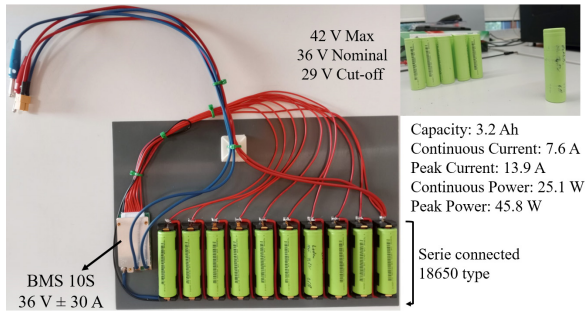

Fig. 6. *Handmade test battery; 36 V nominal / 3.2 Ah capacity*

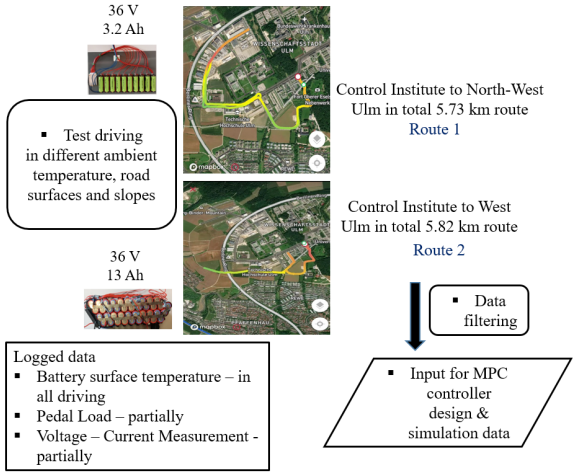

Fig. 7. *Experimental test flow chart*

Fig. 7 explains the workflow during the experimental test driving with both battery types. Fig. 8 shows the general equipment of the test e-bike. The normal bike weighs 30.5 kg, with an additional 30 kg of weight made up of two different gravel sands, each weighing 15 kg. Including driver weights and

the other additional weights, the driving is performed with a total of 137.5 kg.

Fig. 8. *Experimental test boundary condition with 3.2 Ah handmade battery usage*

Fig. 9 shows the battery surface temperature data during test routes recorded at different ambient temperatures with handmade batteries. The maximum slope that exists in this test route is 6 %, and the average slope rate is found to be 2.6 % via GPS data. The drives were performed starting on the 18th of July at 23 °C degree ambient temperature, then continued on July 19th with 28 °C ambient temperature, which was the hottest weather condition in all test drives, then on July 24th at 20 °C, and finalized on July, 26th with 15 °C, which is the coldest weather condition between in all test drives. Fig. 10 shows the colour map taken temperatures vs. time for battery surface temperature based on the different ambient temperatures. Red and blue represent the hottest and coldest temperatures

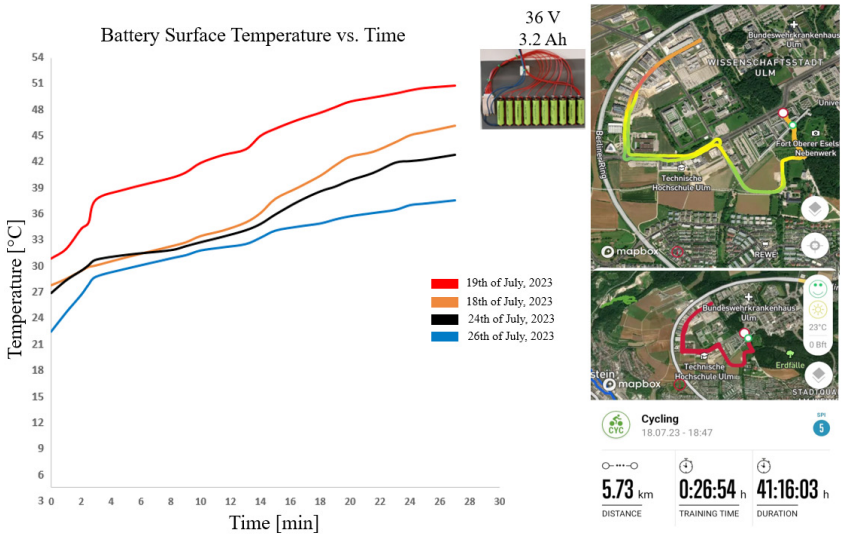

Fig. 9. *Battery surface temperature vs time – handmade battery 3.2 Ah, 5.73 km route north-west Ulm*

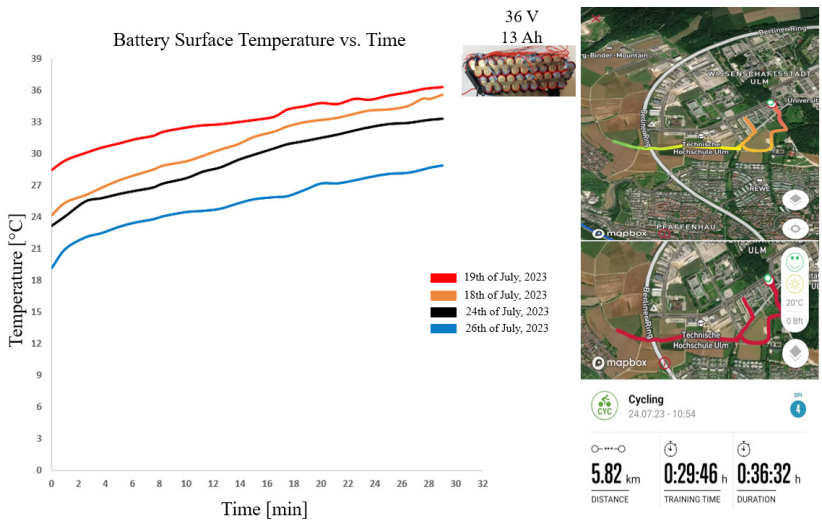

Fig. 10. *Battery surface temperature vs time – e-bike original battery 13 Ah, 5.82 km route west Ulm*

vs the time graph taken by 13 Ah battery capacity. The maximum slope rate in this route is 5 %, and the average slope rate is 2.3 % based on GPS data.

2 PEDAL ACTIVITY vs. VOLTAGE – CURRENT MEASUREMENTS IN HILL-START CONDITION

In this section, the pedal activity vs. voltage [V] and current [I] values are obtained to use these data as MPC model input. Pedal load is the disturbance needed to obtain the target motor torque level. Pedal load creates a disturbance for the desired motor torque level controlled by the thermal MPC battery model, and the pedal load/pedal activity values are measured depending on real-time voltage-current values.

Figs. 11 and 12 show the hill-starting driving conditions in which the voltage-current measurements and pedal load/pedal activity measurements are done simultaneously at 4 % and 6 % incline. Fluctuations occurred in voltage output data due to terminal voltage. Blue represents the terminal voltage; current and pedal activity are defined respectively in orange and black. The hill-starting tests are performed via handmade batteries having a 3.2 Ah capacity. The obtained data are used in Section 4 within Figs. 16 and 17 as powertrain electro-mechanical inputs.

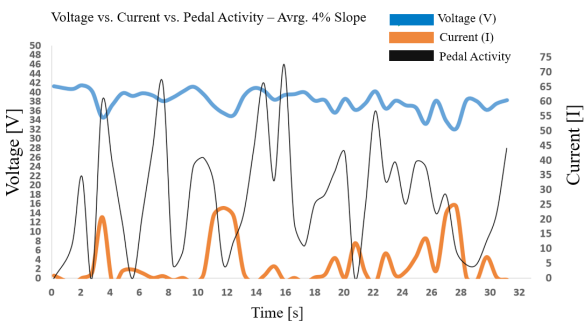

Fig. 11. Real-time voltage – current meas. vs pedal activity on 4 % slope hill driving with handmade battery 3.2 Ah

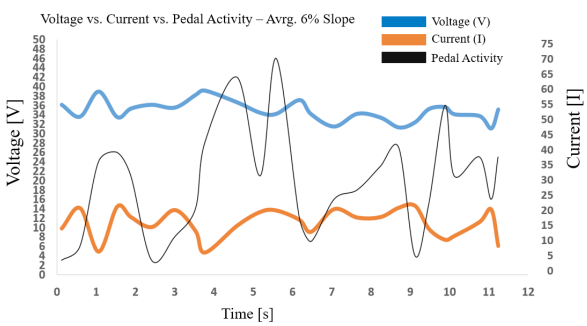

Fig. 12. *Real-time voltage – current meas. vs. pedal activity on 6 % slope hill driving with hand-made battery 3.2 Ah*

3 MPC DESIGN WITH THERMAL AND LONGITUDINAL MODELLING

In this section, the complete cargo e-bike model is modelled based on the experimental test data taken from the field tests. The controller model is designed to be used to provide optimized electric motor energy consumption despite measured disturbances pedal load torque and slope (gradient) torque (Eq. (5)). The generated thermal model is the function of the integrated longitudinal speed control model explained in detail in Section 4. $M\frac{dv}{dt}$ M is the net excitation force obtained after negative forces of Air drag ($F_{Airdrag}$), Slope (F_{Slope}), and Rolling Resistance ($F_{R.Res}$) are removed from total positive forces Electric Motor (F_{Motor}) and Pedal forces (F_{Pedal}).

$$M\frac{dv}{dt} = F_{Motor} + F_{Pedal} - F_{Airdrag} - F_{Slope} - F_{R.Res}. \quad (5)$$

The lumped model is used for the battery thermal model. During experimental tests, surface temperatures are provided via an Arduino thermal datalogger to provide input data for the model. The battery model is also defined as a simple version in Fig. 13. R_i, C_i, and T_i represent the resistance, capacitance, and temperature for the battery's internal region simulated with an electric circuit, and C_S and T_S represent the resistance and capacitance for battery surface in order, and R_A and T_A represent resistance and temperature for ambient conditions.

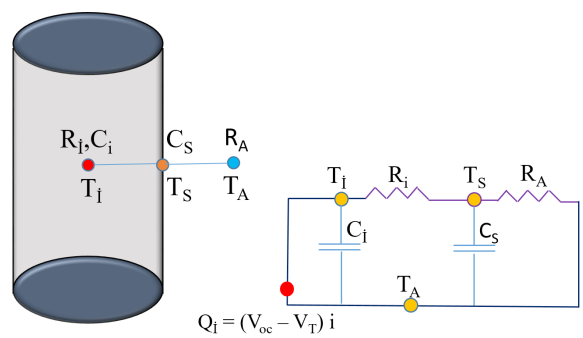

Fig. 13. *Battery thermal lumped model – simplify circuit*

The measured disturbance is ambient temperature, which is the factor for battery surface temperature control [7] and [9]. The reference temperature is the targeted battery surface temperature that can be defined by the model (Fig. 14). The equation of the lumped model defined for this model is shown in Eq. (6).

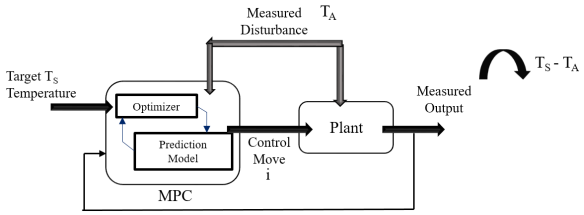

Fig. 14. *MPC battery surface temperature controller algorithm flow*

The terms T_{is} and T_{ss} explain, respectively, the temperature difference between cell internal temperature and ambient temperature ($T_{is} = T_{internal} - T_{ambient}$) and the temperature difference between surface temperature and ambient temperature ($T_{ss} = T_{surface} - T_{ambient}$) represented via measured output (MO) in Fig. 15. In T_{is}, the input heat (generated internal heat) is placed into Eq. (7). The internally generated (Q_i) heat can be defined in Eq. (6). V_{OC} defines the open circuit voltage, V_T is the terminal voltage, and I is the current flow in the circuit. The time-dependent temperature difference between surface and ambient includes radiation heat occurrence created by sun-related emission factor-based heat generation (Q_r) and forced convection heat transfer (Q_{fc}) due to airflow and battery surface contact during movement in an e-bike.

$$Q_i = (V_{OC} - V_T)I, \tag{6}$$

$$\frac{dT_{is}}{dt} = -\frac{1}{R_i C_i}T_{is} + \frac{1}{R_i C_i}T_{ss} + \frac{V_{OC} - V_T}{C_i}I,$$

$$\frac{dT_{ss}}{dt} = -\frac{1}{R_i C_s}T_{is} - \left(\frac{1}{R_i C_s} + \frac{1}{R_0 C_s}\right)T_{ss} + Q_r - Q_{fc}. \tag{7}$$

Eq. (8) shows the state-space model of the thermal lumped model adapted to Li-Ion battery thermal behaviour. The input value is selected as internally generated Heat energy (Q_i). Because the battery surface temperature measurement is easy to measure and gives more accurate data, the output factor is selected as T_{ss}, explaining the temperature difference between the battery surface and ambient (Eq. 9).

$$\begin{bmatrix}\dot{T}_{is}\\ \dot{T}_{ss}\end{bmatrix} = \begin{bmatrix}-\frac{1}{R_i C_i} & \frac{1}{R_i C_i}\\ \frac{1}{R_i C_s} & -\left(\frac{1}{R_i C_s} - \frac{1}{R_0 C_s}\right)\end{bmatrix}\begin{bmatrix}T_{is}\\ T_{ss}\end{bmatrix} + \begin{bmatrix}\frac{V_{oc} - V_T}{C_i}\\ 0\end{bmatrix}[i], \tag{8}$$

$$[T_{ss}] = [0 \quad 1]\begin{bmatrix}T_{is}\\ T_{ss}\end{bmatrix} + [0][V_{OC} - V_T]. \tag{9}$$

Fig. 15 shows the general chart of the MPC integrated battery thermal control model. The target of the model is to allow cargo e-bikes to arrange their surface temperature values based on the experimental field data behaving in experimental-based modelling. The outputs of the battery model are state of charge (SoC) and terminal voltage [V]. MPC controller model is identified with $T_{ambient}$ as measured disturbance (M_D). Reference temperature can be defined by the user to have a safe battery surface temperature. Also, low-temperature occurrence needs low Q_i occurrence, including a reduction in current (I) consumption. The manipulated variable (M_V) is selected as the input of the longitudinal model reference speed belonging to the longitudinal MPC controller **[10]** (Fig. 15).

4 ELECTRIC MOTOR STATE MODEL INTEGRATED LONGITUDINAL SPEED CONTROL MODEL

In this section, the longitudinal speed controller model is explained. The thermal battery MPC controller

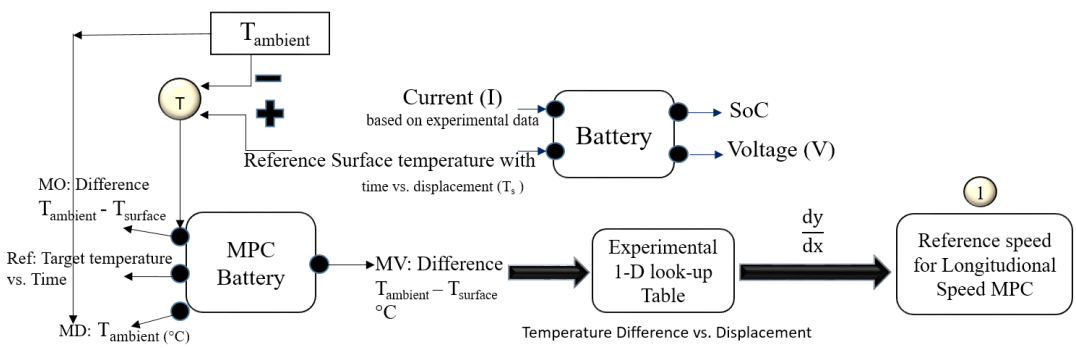

Fig. 15. *MPC battery surface temperature controller via thermal lumped state-space model*

is designed, and M_V is selected as the temperature difference between the battery surface and ambient temperature based on experimental field test data (Fig. 16). Eq. (10) shows the rotational Newton mechanics equation in the driving system. The driving torque equals electric motor (T_m) and pedal sourced torque (T_p) total value minus slope (gradient) torque, air drag force torque (T_A), and rolling resistance (T_R) [11] and [12]. In the force domain, Eq. (5) explains the general equality of the system.

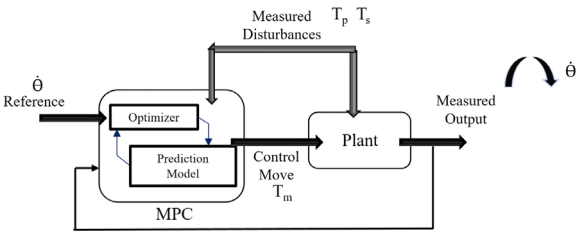

Fig. 16. *MPC longitudinal speed controller algorithm flow*

$$J_x\ddot{\theta} = T_m + T_P - T_S - T_A - T_R. \tag{10}$$

The system is solved based on Newtonian mechanics. To perform this, electric motor torque (T_m) is selected as the control parameter, and pedal torque (T_P) and slope torque (T_S) are selected as measured disturbances [13]. The unmeasured disturbances T_A and T_R are defined by the damping factor multiplied by wheel diameter. b is the equal damping factor, $\dot{\theta}$ is angular velocity obtained by the battery thermal model as experimental field data [14]. J_x is the equal inertia value of the e-cargo bike in pitch movement direction based on cartesian coordinates (Eq. (11)).

$$J_x\ddot{\theta} = -b\dot{\theta}r - T_S - T_m + T_P. \tag{11}$$

Eq. (12) explains the state-space model selected for the longitudinal control model. The state is selected as the angular velocity ($\dot{Q}$) of the electric motor, including the internal reducer. $[B]\times[U]$ matrices are composed of control parameter T_M and measured disturbances T_p and T_S. The output is selected as angular velocity ($\dot{Q}$) compiling $[C]\times[X]$ matrix [15].

$$\dot{x} = \left[\ddot{\theta}\right] = \left[\frac{-br}{J_x}\right]\left[\dot{\theta}\right] + \begin{bmatrix}\frac{1}{J_x} & \frac{1}{J_x} & -\frac{1}{J_x}\end{bmatrix}\begin{bmatrix}T_m\\T_P\\T_S\end{bmatrix},$$

$$y = [1][Q] + \begin{bmatrix}0 & 0 & 0\end{bmatrix}\begin{bmatrix}T_m\\T_P\\T_S\end{bmatrix}. \tag{12}$$

Fig. 17 shows the 1D model of the MPC-integrated longitudinal control chart. In this model, the reference speed ($T_S - T_A$-based speed data from the 1D look-up table, see Fig. 15) is assigned to the battery thermal MPC controller model. MD is selected as pedal torque (T_P) and slope torque (T_S) and linked via Simulink 1D model into the related block. M_O (measured observations) is recorded via GPS speed calculation and converted into angular velocity ($\dot{Q}$) to provide feedback to MPC.

The manipulated variable (M_V) is the selected angular velocity ($\dot{Q}$) which is the input for the 1D look-up table. First, the M_V value is converted into RPM (revolution per minute), and then the RPM vs. motor efficiency table is processed based on the obtained BLDC (brushless direct current) motor data.

5 RESULTS AND DISCUSSIONS

In this section, the control model results obtained in Section 4 are investigated, and the comparison is discussed. The proposed innovative model used in the study is also discussed, and key control parameters and improved outputs are presented.

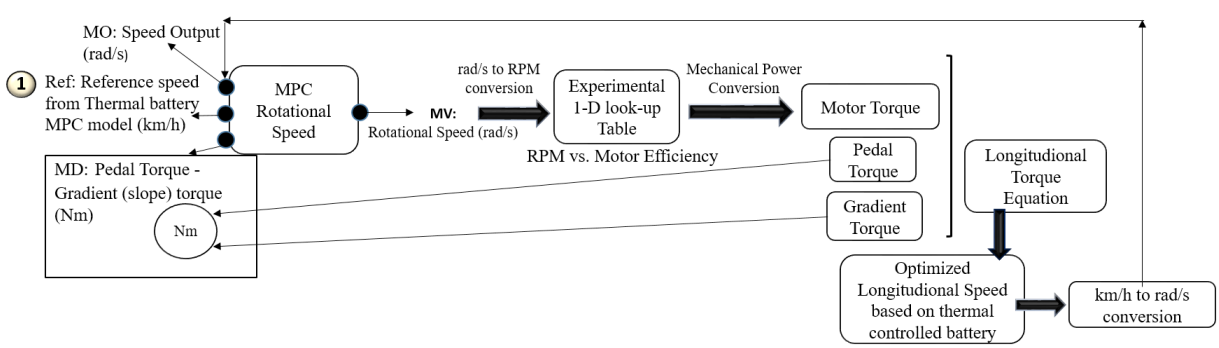

Fig. 17. *MPC longitudinal speed controller 1D model chart via angular to velocity longitudinal converter*

The integrated robust control model with the experimental thermal lumped model approach is shared via step response, temperature sensor data, and dependent motor torque graphs. The model scenarios include the control tuning parameters to have a sensitive battery life cycle and energy consumption against battery thermal ageing.

In model scenario 1, to provide the robust prediction horizon, the weight factor (W_Q) is kept constant, and the thermal and speed control outputs are observed based on 23 due to sensitive step response compared to $\dot{Q}$. In model scenario 2, the input and output weight factors are changed to observe the thermal and speed output behaviours. After the second scenario, the correct weight factor is detected, and the robust control model is provided.

Model Scenario 1

Scenario 1 compares the models as an unconstrained state-space model condition with $W_Q(1)$ = 0.1 Weight factor, $U(1)$ is also measured outputs multiplied with weight factor $W_Q(1)$ (Eqs. (1) and (2)). Eqs. (1) and (2) are the mathematical definition of MPC modelling in Simulink MPC Designer. In this scenario, based on the experimental input data, the prediction horizon effects are investigated to see the over-shoot of the catching reference value in the step response model. The first prediction horizon with the defined weight factors is determined as 10 (Fig. 18); in the next step, the model is run for prediction 23 (Fig. 19). The prediction horizon using $W_Q(1)$ is obtained more stable and robust by using After defining the prediction horizon, the next step is to see the thermal fluctuation by comparing the reference curve obtained from experimental road tests and model results (Fig. 21).

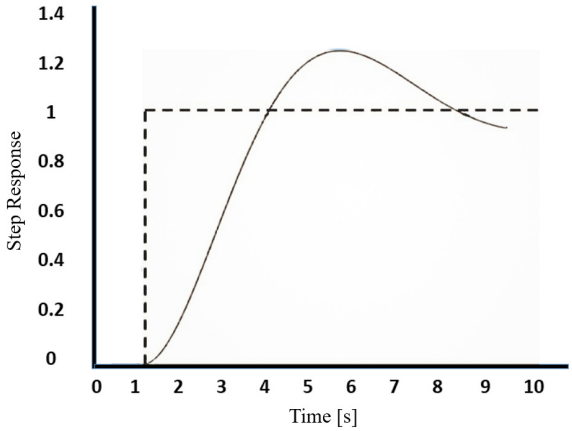

Fig. 18. *Scenario 1. prediction horizon N: 10 vs W_Q: 0.1 – U:1*

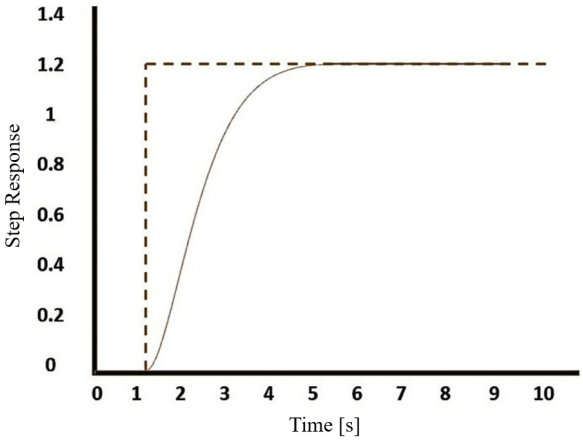

Fig. 19. *Scenario 1. Prediction horizon N: 23 vs W_Q: 0.1 –U:1*

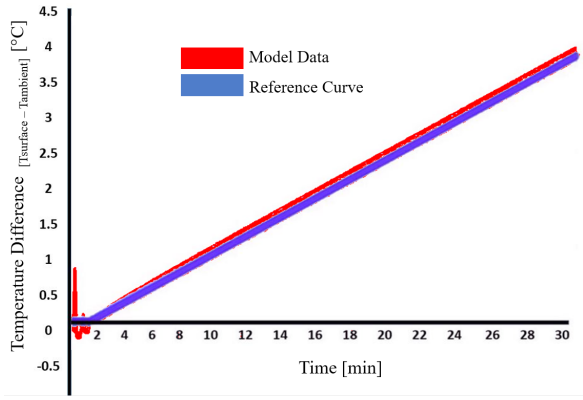

Fig. 20. *Difference between Battery surface temperature and ambient temperature; Blue: Reference curve (from experimental tests shown in Figs. 14 and 15) – Red: Model output*

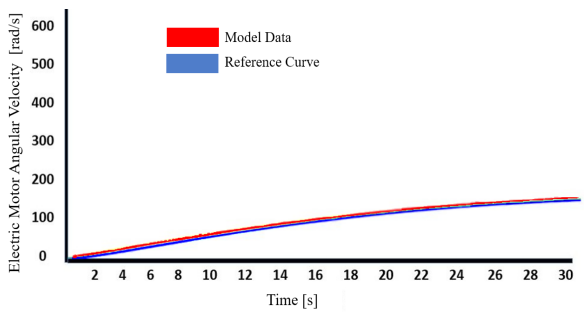

Fig. 21. *Electric motor angular velocity [rad/s] for Model 1; Blue: Reference curve (obtained from the integrated model side; see Figs. 16 and 17) – Red: Model output*

Figs. 20 and 21 show the thermal modelling results and thermally controlled motor angular velocity ($\dot{\theta}$) MPC control data is modelled based on Fig. 19. The green curve represents the reference input in which the target of the temperature difference between the surface and ambient temperature is experimentally obtained from the road tests (Figs. 9

and 10). The control model behaves smoothly starting from the second minute.

The control model is now simulated to investigate motor torque output stability (Fig. 17). The blue curve represents the desired rotational speed, which provides the target longitudinal speed (Fig. 17). The model shows smooth control in rotational angular velocity (Fig. 21) from 0 rad/s to around 100 rad/s during 30 seconds.

Model Scenario 2

Model 2 approaches the model outputs from Weight factor effects. To see the model behaviour, the input weight factor in the model changed to 0.25 $W_Q(2)$ instead of $W_Q(1)$: 0.1 (Scenario 1). The output weight factor is defined as 0.75 $U(2)$. The prediction horizon is kept in Fig. 23, and the model is run (Fig. 22).

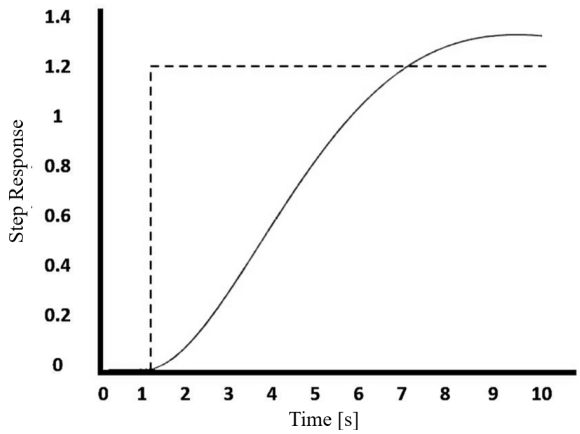

Fig. 22. *Scenario 2. Prediction horizon N: 23 vs. W_Q: 0.25 – U: 0.75*

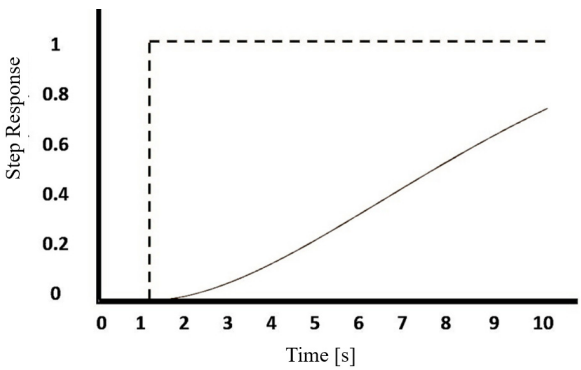

Fig. 23. *Scenario 2. Prediction horizon N: 10 vs W_Q: 0.25 – U: 0.75*

Between Figs. 19 and 22, the overshoot difference is observed in parallel to input and output weight factor changes even in the use of the same prediction horizon. The model outputs on the MPC side show a higher delay in response to input data compared to Scenario 1 (Figs. 18 and 19). Also, the overshoot is prominent compared with Scenario 1 curves. If the prediction horizon goes to 10, the step response drops and delays (Fig. 23).

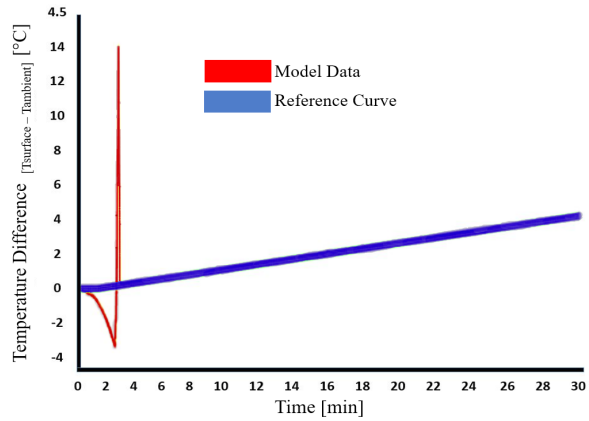

Fig. 24. *Difference between Battery surface temperature and Ambient temperature; Blue: Reference curve (from experimental tests shown in Figs. 14 and 15) – Red: Model output*

Fig. 24 shows the difference between the battery surface temperature and ambient temperature during 30 minutes, similar to the experimental tests. As seen in around two seconds, the measured outputs (in yellow) present prominent overshoot values compared to Fig. 20. Fig. 25 is the angular velocity data providing longitudinally measured outputs. Similar to the thermal model, around two seconds, the over-shoot occurs; after this time range, up to 30 seconds, the smooth correlation is observed. Compared to Fig. 21, the weight factor is observed with higher overshoot also in rotational motor speed control integrated with the MPC thermal battery model.

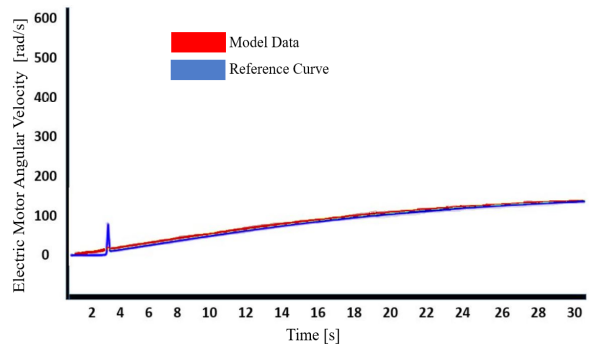

Fig. 25. *Electric motor angular velocity [rad/s] for Model 2; Blue: Reference curve (obtained from the integrated model side; see Figs. 16 and 17) – Red: Model output*

6 CONCLUSION

In this study, a cargo e-bike is investigated based on thermal and longitudinal control with MPC control design to provide optimal motor torque generation in pedal assist system (PAS) used plants. The field tests are performed via batteries with different capacities to show internal resistance-based surface temperature. Then, the desired thermal conditions are defined as a function to provide robust control for longitudinal speed control subjecting to uncertain road disturbances. The target of the integrated robust control model is constructed based on the thermal lumped model approach by predicting compulsive road disturbances under a weight load. The new model is based on the uncertain experimental road data configured with the MPC controller, in which the battery and longitudinal robust control have been designed for the three-wheeler cargo e-bike. The model is developed based on experimental test data by measuring the thermal conditions of Li-Ion batteries and pedal load vs. voltage-current input data for electro-mechanical model development. To cover the sensitivity, the most used battery energy capacities are selected to create reference curves and avoid uncertainty.

The weight factor and prediction horizon selection sensitivities are comparatively investigated to increase robustness in the developed model. In this direction, the performance of the control model can be controlled within the simulation phase. During the control model simulations, the step response, thermal model, and integrated rotational motor speed are observed for 10 seconds, 30 minutes, and 30 seconds, respectively, to create a similar environment to the experimental tests. The model also presents a cost-effective methodology by giving life-expansion possibilities for Li-Ion batteries. In addition, the proposed control model can be performed and analysed on fully electrified e-micromobility vehicles in which the battery thermal conditions and cost-effectiveness are concerned.

7 ACKNOWLEDGEMENT

This study is funded by TUBITAK 2219 (The Scientific and Technological Research Council of Turkey) entitled 'An Experimental Battery Model Development for PAS (Pedal Assist System) of E-Quadricycle under Hill Hybrid Driving Modes at Different Ambient Temperatures'. The author is extremely grateful to the 'Institute of Measurement, Control, and Microtechnology, Ulm University, Germany' for supporting the research project and providing testing opportunities.

8 NOMENCLATURES

T_{is}	battery temperature difference, $T_{internal} - T_{ambient}$, [°C]
T_{ss}	battery temperature difference, $T_{surface} - T_{ambient}$, [°C]
Q_i	battery internally generated heat, [J]
V_{OC}	open circuit voltage, [V]
Q_r	radiation-based heat, [J]
Q_{fc}	forced convection heat, [J]
T_m	cargo e-bike electric motor torque, [N·m]
T_P	cargo e-bike driver pedal-generated torque, [N·m]
T_S	gradient based negative slope torque, [N·m]
T_A	aerodynamic drag based negative torque, [N·m]
T_R	road based negative rolling resistance torque, [N·m]

9 REFERENCES

[1] Masti, D., Bemporad, A. (2018). Learning nonlinear state-space models using deep autoencoders. *IEEE Conference on Decision and Control*, p. 3862-3867, **DOI:10.1109/CDC.2018.8619475**.

[2] Zamarreño, J.M., Vega, P., García, L.D., Francisco, M. (2000). State-space neural network for modelling, prediction and control. *Control Engineering Practice*, vol. 8, no. 9, p. 1063-1075, **DOI:10.1016/S0967-0661(00)00045-9**.

[3] Ma, H., Pei, W., Zhang, Q. (2022). Battery energy consumption analysis of automated vehicles based on MPC trajectory tracking control. *Electrochem*, vol. 3, no. 3, p. 337-346, **DOI:10.3390/electrochem3030023**.

[4] Surya, S., Samanta, A., Marcis, V., Williamson, S. (2021). Smart core and surface temperature estimation techniques for health-conscious lithium-ion battery management systems: A model-to-model comparison. *Energies*, vol. 15, no. 2, 623, **DOI:10.3390/en15020623**.

[5] Batiyah, S., Sharma, R., Abdelwahed, S., Alhosaini, W., Aldosari, O. (2022). Predictive control of PV/battery system under load and environmental uncertainty. *Energies*, vol. 15, no. 11, 4100, **DOI:10.3390/en15114100**.

[6] Masoudi, A., Azad, N.L. (2017). MPC-based battery thermal management controller for plug-in hybrid electric vehicles. *IEEE American Control Conference*, p. 4365-4370, **DOI:10.23919/ACC.2017.7963627**.

[7] Shi, H., Wang, L., Wang, S., Fernandez, C., Xiong, X., Dablu, B.E., Xu, W. (2022). A novel lumped thermal characteristic modeling strategy for the online adaptive temperature and parameter co-estimation of vehicle Lithium-Ion batteries. *Journal of Energy Storage*, vol. 50, 104309, **DOI:10.1016/j.est.2022.104309**.

[8] Tatjewski, P. (2017). Offset-free nonlinear model predictive control with state-space process models. *Archives of Control Sciences*, vol. 27, no. 4, p. 595-615, **DOI:10.1515/acsc-2017-0035**.

[9] Kirchgässner, W., Wallscheid, O., Böcker, J. (2023). Thermal Neural networks: Lumped-parameter thermal modeling with

state-space machine learning. *Engineering Applications of Artificial Intelligence*, vol. 117, 105537, **DOI:10.1016/j.engappai.2022.105537**.

[10] Yao, Q., Tian, Y. (2019). A model predictive controller with longitudinal speed compensation for autonomous vehicle path tracking. *Applied Sciences*, vol. 9, no. 22, 4739, **DOI:10.3390/app9224739**.

[11] Ho, P.J., Yi, C.P., Lin, Y.J., Chung, W.D., Chou, P.H., Yang, S.C. (2023). Torque measurement and control for electric-assisted bike considering different external load conditions. *Sensors*, vol. 23, no. 10, 4657, **DOI:10.3390/s23104657**.

[12] Rokonuzzaman, M., Mohajer, N., Nahavandi, S., Mohamed, S. (2021). Model predictive control with learned vehicle dynamics for autonomous vehicle path tracking. *IEEE Access*, vol. 9, p. 128233-128249, **DOI:10.1109/access.2021.3112560**.

[13] Maceira, D., Luaces, A., Lugris, U., Naya, M.Á., Sanjurjo, E. (2021). Roll angle estimation of a motorcycle through inertial measurements. *Sensors*, vol. 21, no. 19, 6626, **DOI:10.3390/s21196626**.

[14] Cui, D., Wang, G., Zhao, H., Wang, S. (2020). Research on a path-tracking control system for articulated tracked vehicles. *Strojniški vestnik - Journal of Mechanical Engineering*, vol. 66, no. 5, p. 311-324, **DOI:10.5545/sv-jme.2019.6463**.

[15] Pai, S., Neuberger, B., Buchholz, M. (2021). Adaptive model predictive stabilization of an electric cargo bike using a cargo load moment of inertia estimator. *Automatisierungstechnik*, vol. 69, no. 7, p. 632-642, **DOI:10.1515/auto-2021-0032**.